

SNS Magnet 3D-Simulations at ORNL

J. G. Wang

Abstract:

This note is prepared for a presentation at a special mini-workshop on magnet simulations for particle accelerators during PAC05. It summarizes the magnet 3D-simulation activities at ORNL and highlights our simulation results for a few SNS magnets. The 3D-simulations at ORNL have been performed to guide magnet tests for the search coil design and measurement data verification; to study more detailed field distributions for further beam dynamics analysis; and to investigate magnetic fringe fields and interferences in the SNS ring. The motivation and applications of our simulation work at ORNL are described with a few examples.

Key words: Magnet simulations, Magnetic dipole and quadrupole, Integrated field and gradient, 3D-multipole contents, Magnetic fringe field, Magnetic interference or crosstalk

1. Introduction

The SNS accelerator consists of more than 30 different kinds of magnets with a total number of more than 600. These magnets include electro-magnetic dipoles, quadrupoles, sextupoles, and other correctors. All these magnets were designed by our partner labs, namely, LBNL, LANL, and BNL, where extensive design simulation activities were involved.

At ORNL we started to build a magnet measurement lab a few years ago to test the SNS magnets for its linac and transfer lines. We realized that 3D magnet simulations at ORNL were still necessary for accomplishments of our tasks, such as for the tests of 8D533, 12Q45, 8Q35, 21Q40 etc. Indeed, we have greatly benefited from our simulation work in the assistance and guidance of magnet measurements. In the mean while, per the request of Accelerator Physics Group, we have performed 3D-simulation of the injection chicane dipoles (D2 & D3). The simulation has provided not only the 3D magnetic field distributions in grids, but also led to a magnetic 3D-multipole expansion, which reveals more insight into the magnet physics and is the basis for beam optics analysis. At this time we continue 3D magnet simulations to study magnetic fringe fields and magnetic interferences in the ring doublets. This work should provide useful information for the ring commissioning and operation.

We have so far simulated nine SNS magnets including 8D533, 12Q45, 8Q35, 21Q40, 17D120, 24D70 & 24D48, 30Q58 & 30Q44. We plan to simulate 17D244 in near future in connection with our test of this big dipole. We also plan to simulate 26Q40 and a few correctors in future, thus we will have complete simulation files for the SNS ring and transfer line lattice magnets. A list of the SNS magnet simulations at ORNL can be found in Table 1.

The magnetic simulation code we employ is OPERA/TOSCA [1], starting from version 8.0 several years ago up to version 10.01 today. The procedure involves basically four steps: build model, generate mesh, solve problem, and analyze results. The magnet models in simulations are built by an OPERA package “Pre-processor” or “Modeller”. The mesh generator then produces the surface and volume meshes. The magneto-static problem is solved by TOSCA to produce output files, which are used by the OPERA Post Processor to analyze and yield desired results. We began our simulations with the “Pre-processor” to build models for three magnets: 8D533, 12Q45, and 21Q40. We then have switched to the “Modeller” for other magnets, which employs a modularized approach and is especially suited to simulate two or more magnets together.

This note highlights our 3D-simulation applications in three areas: assistance to magnetic measurements, study of magnetic field distribution and 3D-multipoles, investigation of magnetic fringe fields and interferences. In Section 2 we describe how the simulation of 8D533 guided our measurement of this big dipole. Section 3 provides a brief description of the simulation and multipole expansion of the chicane dipoles D2 & D3. In Section 4, we present the preliminary results of magnetic fringe fields and interferences in the ring straight section assemblies (30Q58 & 30Q44 plus 41CD30). A brief summary follows in Section 5.

Table 1 SNS magnet 3D-simulations at ORNL

	B	C	D	E	G	H
1	Location	Magnet Type	Designation	Design	3D Simulations @ ORNL	
2						
4	MEBT	Quad	R16QN45	LBNL		
6	DTL	EMD		LANL		
7		PMQ				
9	CCL	Quad	R175QN45	LANL		
10		Quad	R177QN80			
11		Quad	R24QN80			
13	SCL	Quad	8Q35	LANL	Yes	5. For measurement
15	HEBT	Dipole	8D533	BNL	Yes	1. For measurement
16		Dipole	8D406			
17		Quad	12Q45		Yes	2. For measurement
18		Quad	21Q40		Yes	3. For measurement
19		Correctors			
21	Ring	Dipole	17D120	BNL		
22		Dipole	24D64			
23		Dipole	24D70		Yes	4. For field distributions
24		Dipole	24D48			
25		Dipole	24D68			
26		Quad	21Q40		Yes	
27		Quad	26Q38			
28		Quad	30Q44			
29		Quad	30Q58		Yes	6. For magnetic crosstalk
30		Correctors			
31		Injection kick				
32		Injection Septum				
33	Extraction kick					
34	Extraction Septum					
36	RTBT	Dipole	17D244	BNL	Planed	7. For measurement
37		Dipole	22DV50			
38		Quad	21Q40		Yes	4. For measurement
39		Quad	30Q44			
40		Quad	30Q58		Yes	
41		Quad	36Q85			
42		Correctors			

2. 3D-simulations for 8D533 measurements

There was no accelerator magnet related program at ORNL when the SNS project started. In 2000 a decision was made to establish a magnet measurement lab on the SNS site for the tests of the SNS linac and transfer line magnets. A HEBT dipole (8D533) was the first SNS magnet being tested at ORNL. The magnet was designed by BNL as a C-shaped dipole in order to use their opening side for beam energy filtering. The C-shaped electromagnetic dipoles always have a non-uniform field distribution in the gap. The main constituent of this non-uniformity is a quadrupole gradient. The design called for the field non-uniformity less than 1/1000 for the SNS transfer line. The main goal of tests was to measure the field non-uniformity in the gap [2-4].

We started from scratch to build our test system consisting of magnet support platform, search coil, electronics equipment, control and analysis software, etc. Since 8D533 dipole is more than 5 m long, we decided to employ a translational coil, rather than conventional rotating coils, in order to ease mechanical difficulties. A photo of 8D533 test setup is shown in Fig. 1.



Fig. 1 Layout of HEBT dipole 8D533 tests.

When we started to design the translational coil, which had a narrow rectangular shape of 6.3 m in length and about 1 cm in width, a natural question was the integrated non-uniformity and expected signal from our test system. We realized that 3D simulation of the dipole was a necessity to accomplish our task. That was the original motivation of our 3D-simulation work: to guide the design of the test system and to provide an expected signal from simulation. The 3D-simulation model of 8D533 and its integrated field distribution is shown in Figs. 2 and 3. According to Fig. 3, we designed the search coil and expected an output signal from an electronic integrator as shown in Fig. 4.

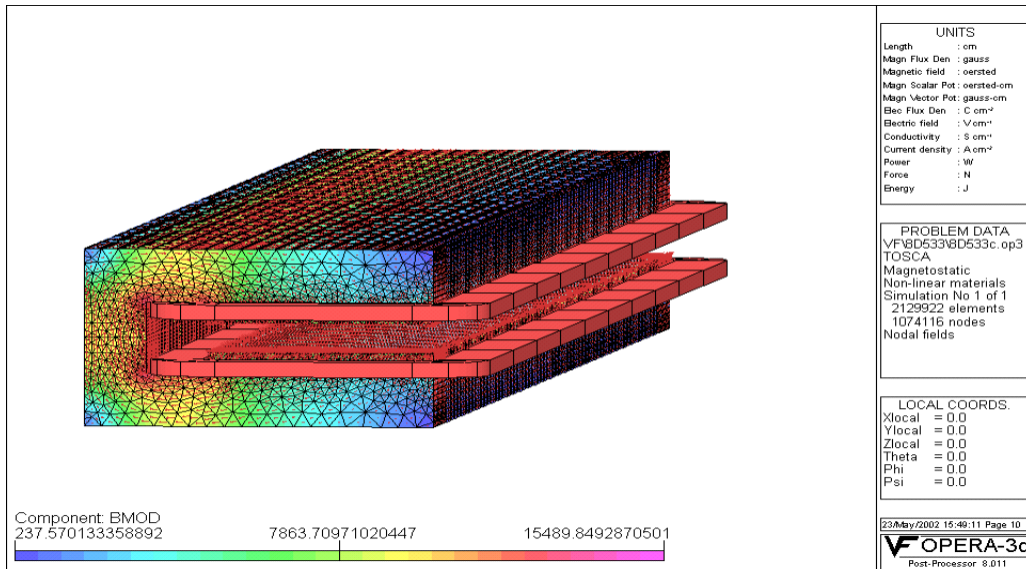


Fig. 2 8D533 model in 3D-simulation.

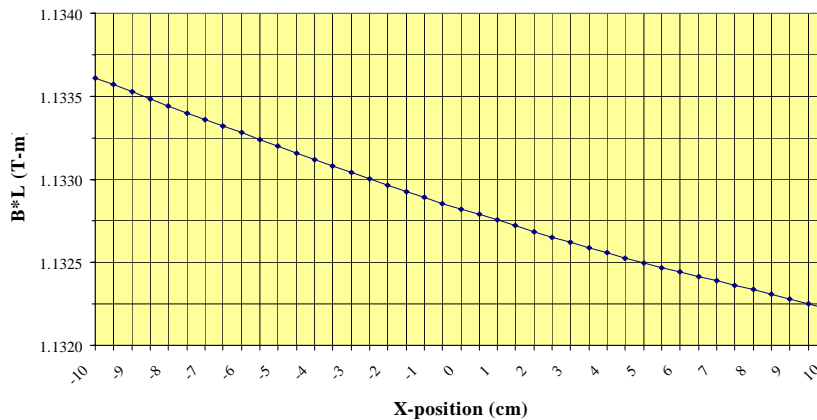


Fig. 3 Integrated field non-uniformity across 8D533 gap.

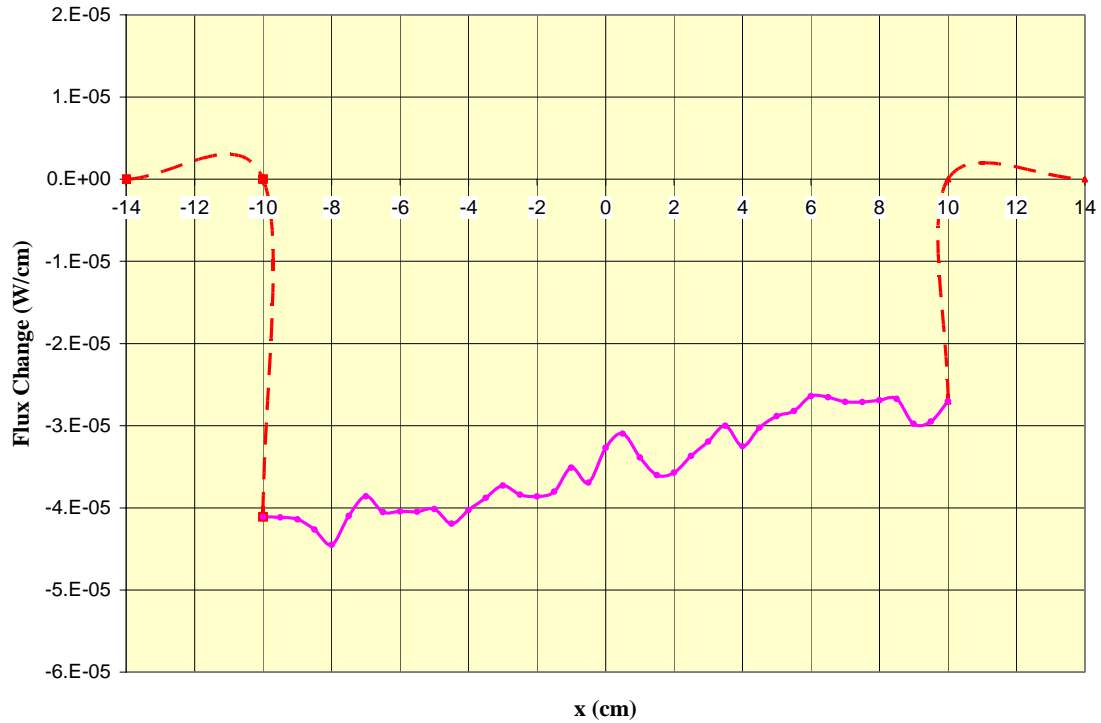
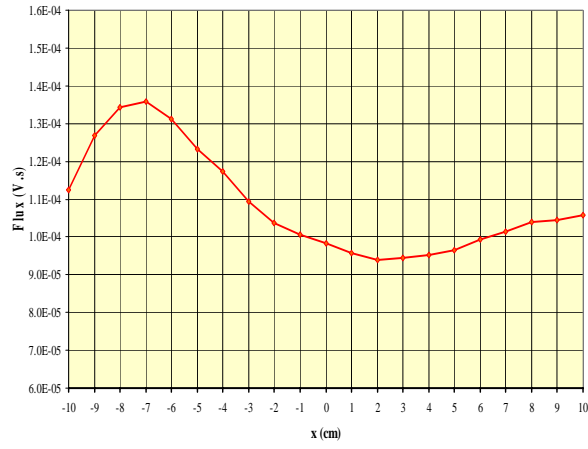


Fig. 4 Expected output signal by simulation where the dashed lines are rather arbitrary.

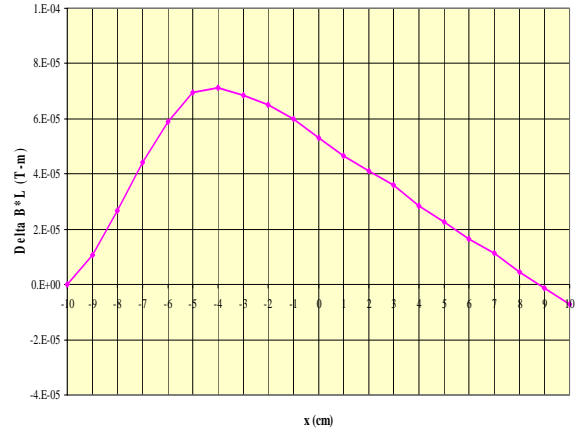
When we started the experiment, there were many problems in a newly established test system, and the output signal was quite different from the simulation predictions for quite a while. A few examples are shown in Fig. 5 (1)-(6), where the left row depicts the electrical signal from the integrator, while the right row gives the corresponding non-uniformity of the dipole. Since we had expectations as shown in Figs. 3 & 4 from simulation, it would be a little easier to trouble-shooting our test system. For example, from Fig. 5(2) to Fig. 5(3) we found that we mistakenly used a stationary bucking winding, which caused induced signal through mutual inductance of two windings; from Fig. 5(3) to Fig. 5(4) we realized the importance of correctly handling a pedestal of the integrator. Figure 5(5) shows the correct result, but still somewhat different from the simulation prediction. Thus, an independent measurement of the non-uniformity by a tesla meter was performed to support the data from the translational coil measurement. It was sometime later, we found that the non-uniformity of the dipole depends on the maximum current during cycling procedures [3]. Figure 5(6) shows that we could reach good agreement between measurement and simulation, and we could even improve the non-uniformity with this method.

(1)

8D533 Output Signal (11_02_2001)

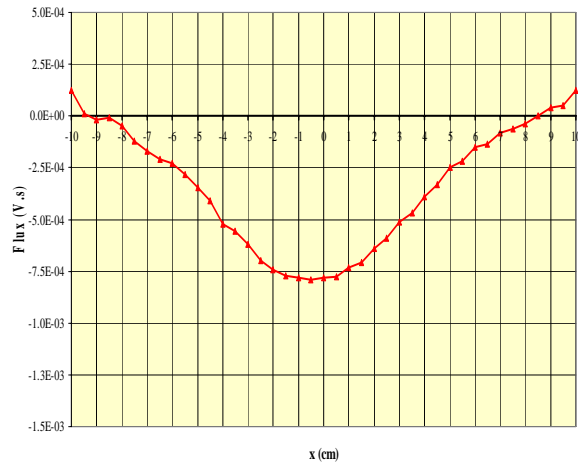


8D533 Non-Uniformity (11_02_2001)



(2)

8D533 Output Signal (11_14_3_2001)

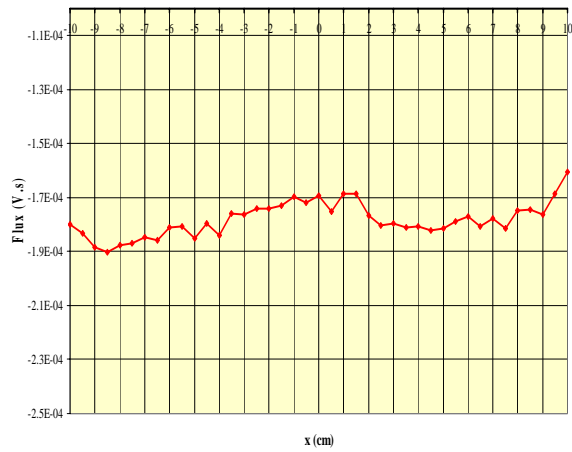


8D533 Non-Uniformity (11_14_3_2001)

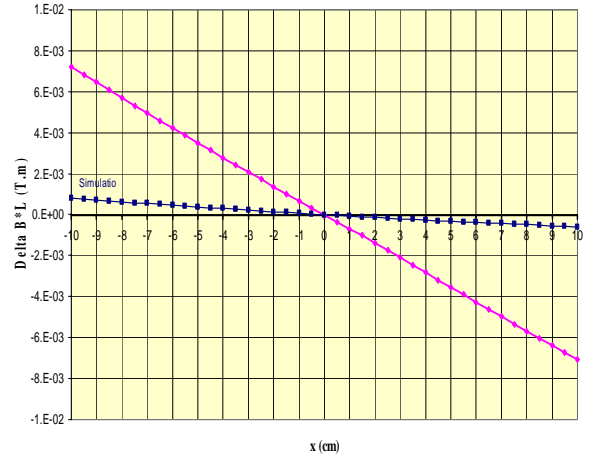


(3)

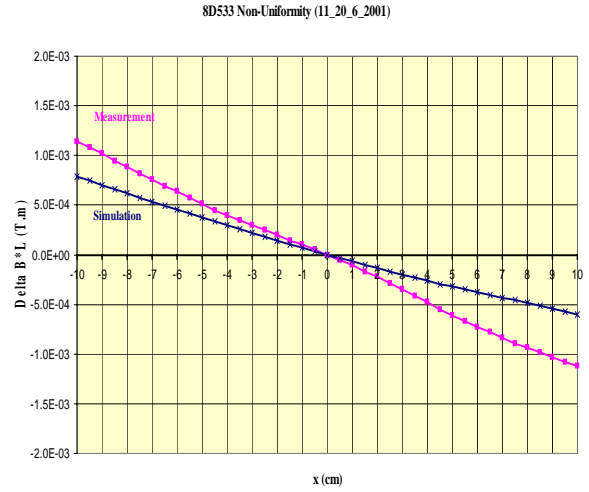
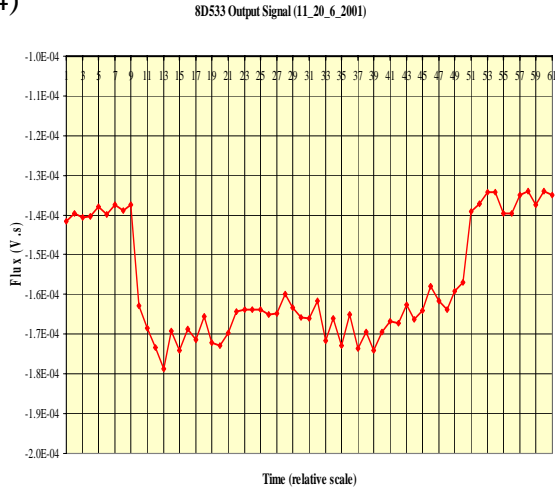
8D533 Output Signal (11_15_11_2001)



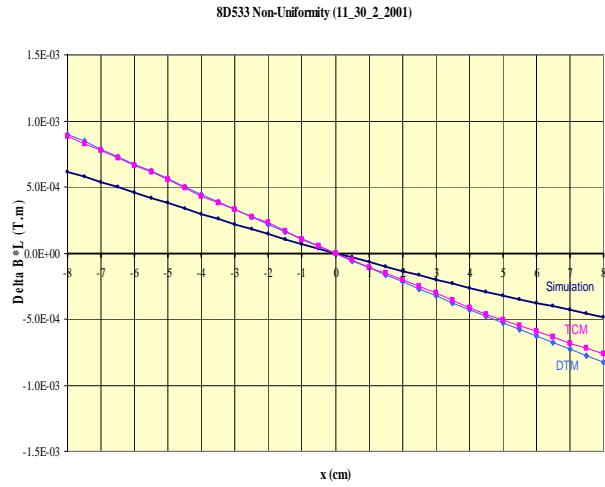
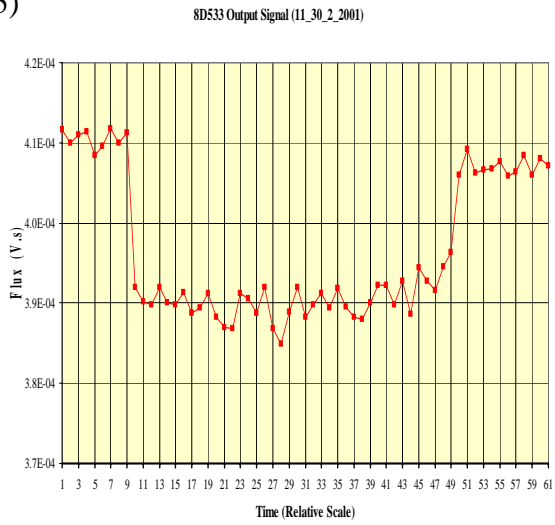
8D533 Non-Uniformity (11_15_11_2001)



(4)



(5)



(6)

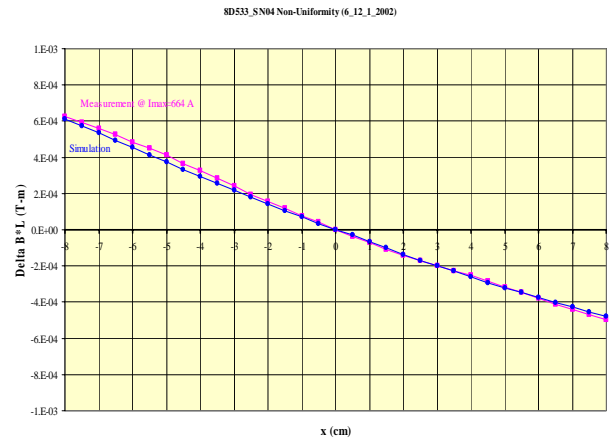
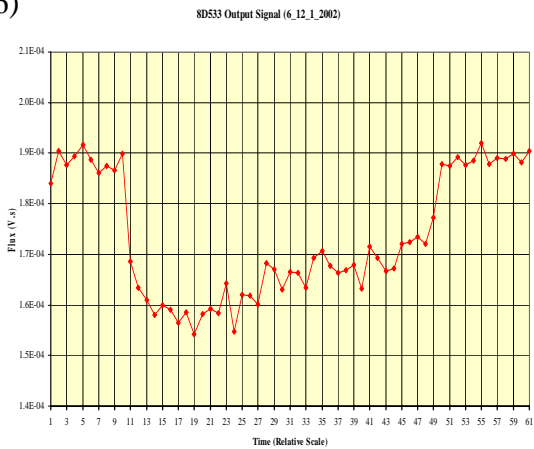


Fig. 5 Output signal of integrator (left) and its resulted “field non-uniformity” (right).

3. Field distributions of chicane dipoles D2 & D3

SNS ring injection employs four chicane dipoles (D1-D4) to control beam orbit. The stripping foil is located on the edge of D2. Its field distribution is critical to H⁻ beam stripping, stripped electron collection, and circulating proton beam. The chicane dipoles were designed by BNL and their simulation files do exist [5]. In order to study beam dynamic issues in the injection region, we believed it would be more convenient to have the simulation work at ORNL. Since D3 is close to D2, and the two dipoles have complementary pole tip structures, it is natural to simulate the two dipoles together [6].

We use the package “Modeller” of OPERA3d to build the models for D2 and D3 separately first for simulations and then to combine them together for final simulation, as shown in Fig. 6. The axial field distribution of these two dipoles is plotted in Fig. 7. The simulation also has produced three dimensional field distributions on grids for beam tracking and other applications.

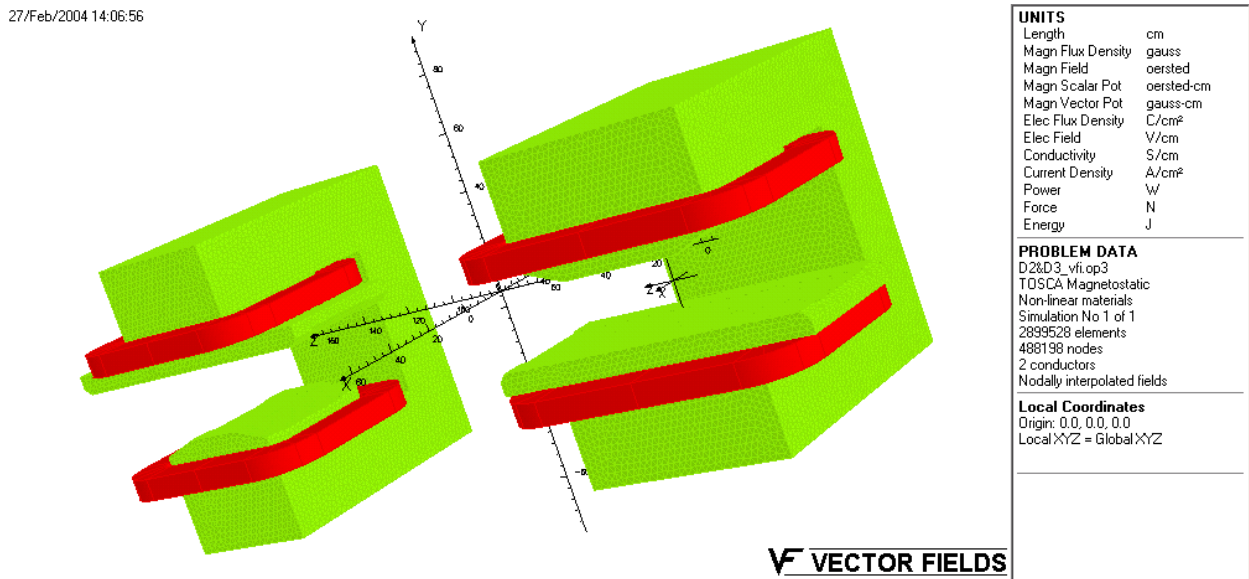


Fig. 6 Simulation model of chicane dipoles D2 & D3.

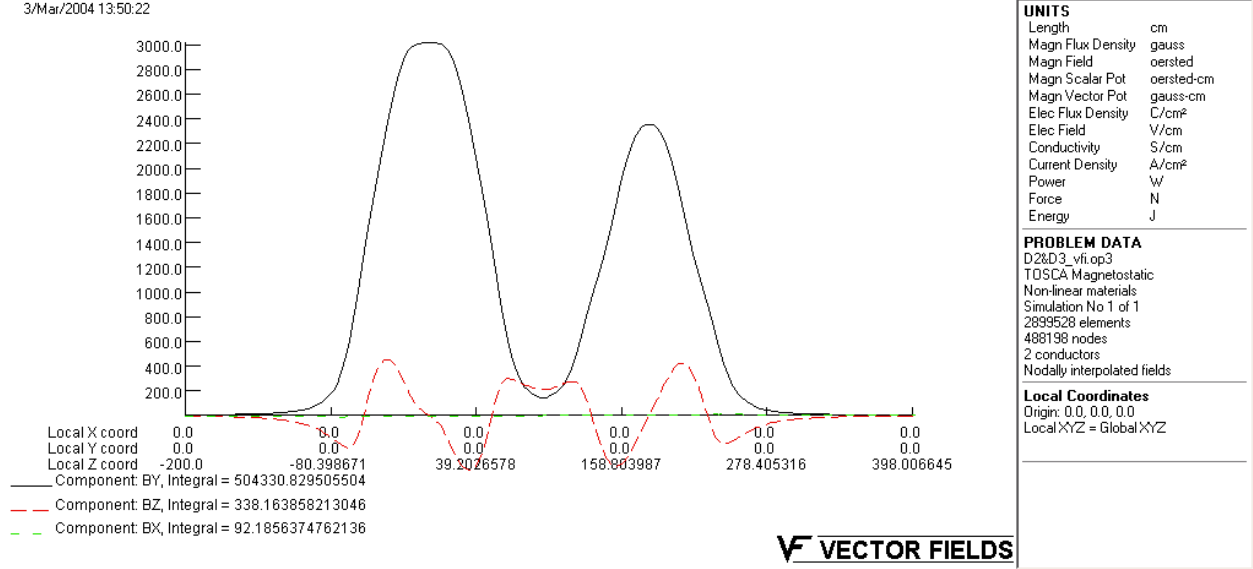


Fig. 7 Axial field distribution of chicane dipoles D2&D3 from simulation.

3D field distribution data on grids from simulations have some disadvantages in applications. The first one is the large memory size, which makes difficult to store and manage the data. In this case, for a rectangular bar of 20x20x600 cm³ with a step size of 0.5 cm, the data take a memory size of about 250 MB. The second problem is that discrete data points do not provide any insight into the magnet physics, and by using them we never know to what level of accuracy the beam optics is analyzed. A remedy for these problems is to make a 3D multipole expansion based on simulation data, as sketched below.

First, from OPERA3d post processor we calculate and Fourier-decompose a field component, say B_r , on the surface of a cylinder of radius R , co-axial with the magnet axis:

$$B_r(R, \theta, z) = \sum_{m=0}^{\infty} \mathcal{B}_m(R, z) \sin(m\theta) + \mathcal{A}_m(R, z) \cos(m\theta).$$

We then can obtain the generalized gradients according to

$$C_{m,s}(z) = \frac{1}{2^m m!} \frac{1}{\sqrt{2\pi}} \int_{-\infty}^{\infty} dk \exp(ikz) \frac{k^{m-1}}{I_m'(kR)} \tilde{\mathcal{B}}_m(R, k),$$

$$C_{m,c}(z) = \frac{1}{2^m m!} \frac{1}{\sqrt{2\pi}} \int_{-\infty}^{\infty} dk \exp(ikz) \frac{k^{m-1}}{I_m'(kR)} \tilde{\mathcal{A}}_m(R, k).$$

Here $\tilde{\mathcal{B}}_m(R, k)$ and $\tilde{\mathcal{A}}_m(R, k)$ are the Fourier transforms of $\mathcal{B}_m(R, z)$ and $\mathcal{A}_m(R, z)$, and $I_m(x)$ is the modified Bessel function of the first kind of order m .

The field components at any point within the cylinder can be constructed as

$$B_r = \sum_{m=0}^{\infty} \sum_{\ell=0}^{\infty} (-1)^{\ell} \frac{m!(2\ell+m)}{2^{2\ell} \ell!(\ell+m)!} C_{m,\alpha}^{[2\ell]}(z) r^{2\ell+m-1} \begin{Bmatrix} \text{Sin}(m\theta) \\ \text{Cos}(m\theta) \end{Bmatrix},$$

$$B_{\theta} = \sum_{m=0}^{\infty} \sum_{\ell=0}^{\infty} (-1)^{\ell} \frac{m!m}{2^{2\ell} \ell!(\ell+m)!} C_{m,\alpha}^{[2\ell]}(z) r^{2\ell+m-1} \begin{Bmatrix} \text{Cos}(m\theta) \\ -\text{Sin}(m\theta) \end{Bmatrix},$$

$$B_z = \sum_{m=0}^{\infty} \sum_{\ell=0}^{\infty} (-1)^{\ell} \frac{m!}{2^{2\ell} \ell!(\ell+m)!} C_{m,\alpha}^{[2\ell+1]}(z) r^{2\ell+m} \begin{Bmatrix} \text{Sin}(m\theta) \\ \text{Cos}(m\theta) \end{Bmatrix}.$$

Here α is either s for the sine term or c for the cosine term.

The correctness of the 3D multipole expansion can be easily verified by comparing the on-axis gradients from the expansion to the on-axis field directly obtained from the simulation data. These are shown in Figs. 8-10 for B_y , B_z , and B_x . The agreement is very good.

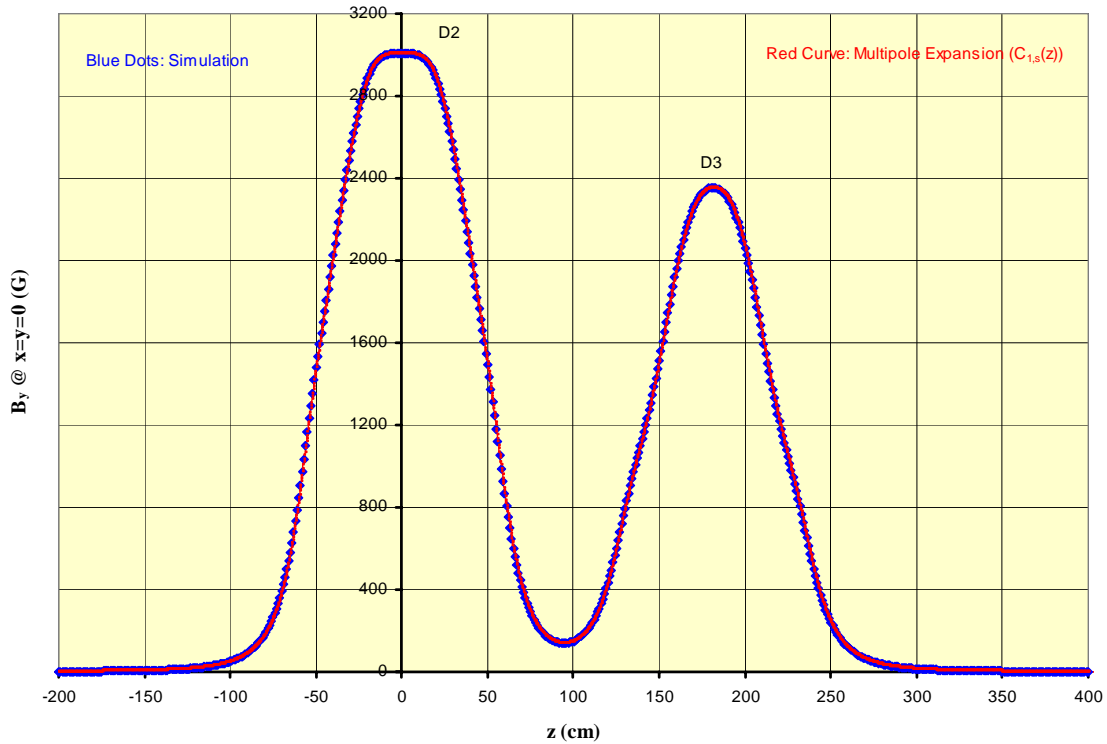


Fig. 8 B_y at $x=y=0$ versus z .

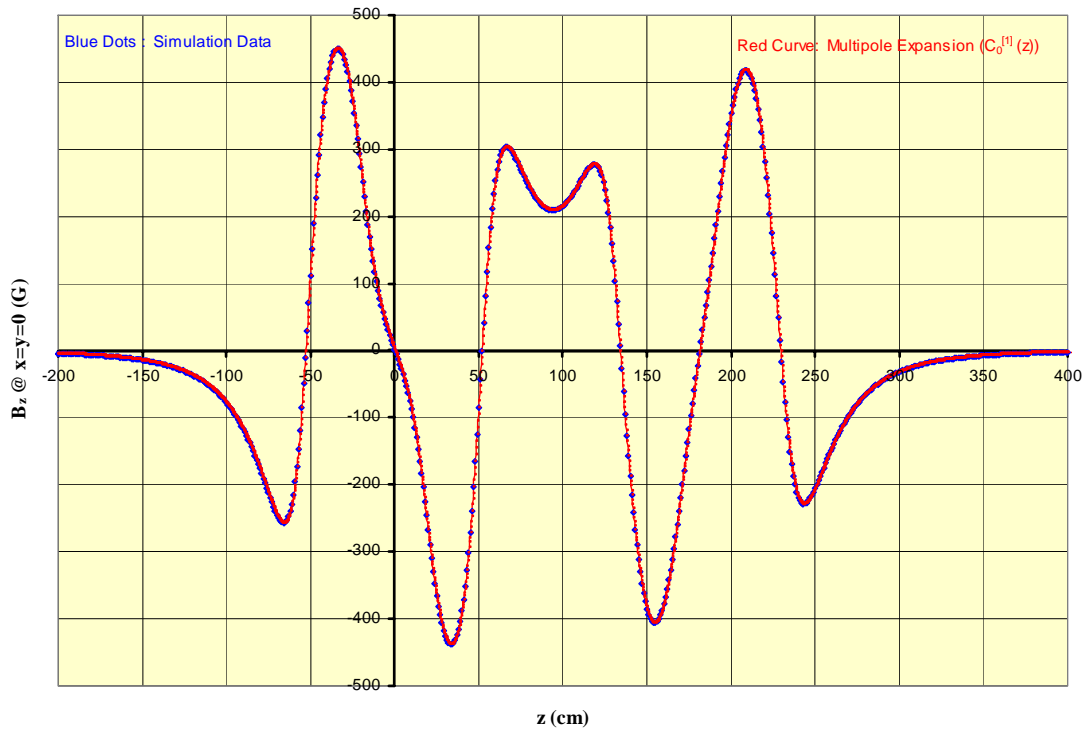


Fig. 9 B_z at $x=y=0$ versus z .

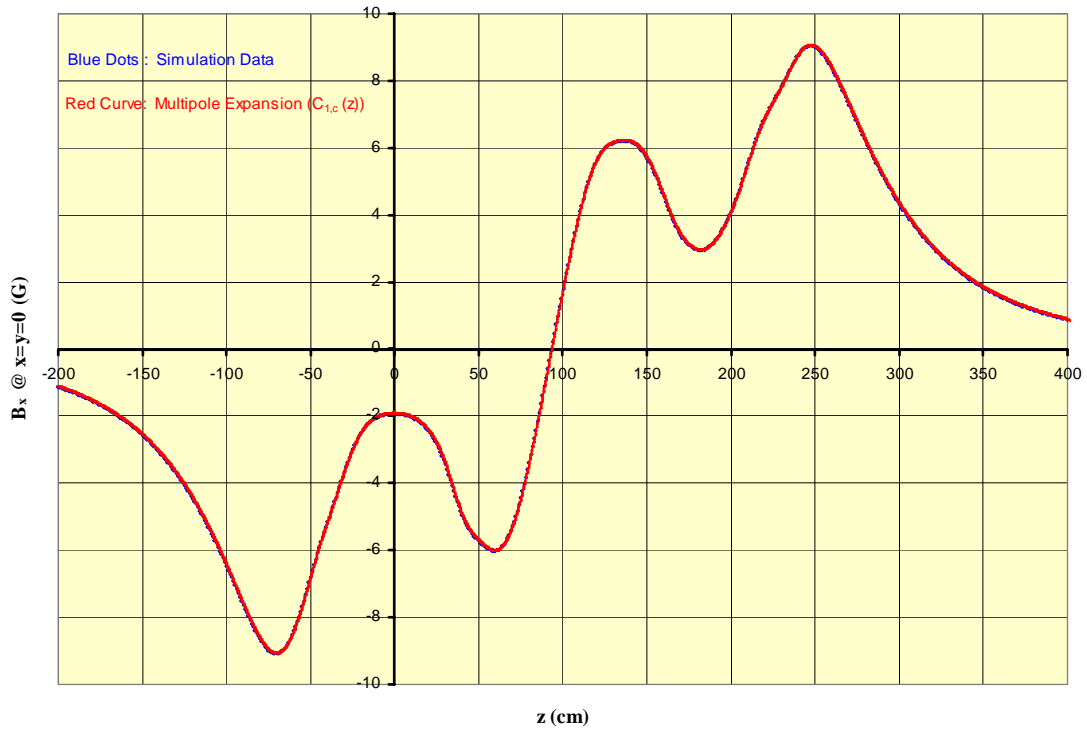


Fig. 10 B_x at $x=y=0$ versus z .

The magnetic field at any point inside the cylinder can be calculated from the generalized gradients. In practice, a cut to a certain order has to be made. A 5th-order representation of the magnetic field covers the multipoles up to the regular dodecapoles and pseudo-dodecapoles. The explicit expressions for this representation are given below. A comparison between the expansion results and the simulation data are shown in Figs. 11-14. In general, the agreement is very good for small radius. When it is far away from the axis, the discrepancy may get larger, and higher-order terms, such as up to 9th order, is required for better agreement, as shown in Fig. 14.

$$\begin{aligned}
B_r = & \left[-\frac{1}{2} C_0^{[2]} r + \frac{1}{16} C_0^{[4]} r^3 - \frac{1}{384} C_0^{[6]} r^5 + \dots \right] + \\
& + \left[C_{1,s} - \frac{3}{8} C_{1,s}^{[2]} r^2 + \frac{5}{192} C_{1,s}^{[4]} r^4 - \dots \right] \sin(\theta) + \left[C_{1,c} - \frac{3}{8} C_{1,c}^{[2]} r^2 + \frac{5}{192} C_{1,c}^{[4]} r^4 - \dots \right] \cos(\theta) + \\
& + \left[2C_{2,s} r - \frac{1}{3} C_{2,s}^{[2]} r^3 + \frac{1}{64} C_{2,s}^{[4]} r^5 - \dots \right] \sin(2\theta) + \left[2C_{2,c} r - \frac{1}{3} C_{2,c}^{[2]} r^3 + \frac{1}{64} C_{2,c}^{[4]} r^5 - \dots \right] \cos(2\theta) + \\
& + \left[3C_{3,s} r^2 - \frac{5}{16} C_{3,s}^{[2]} r^4 + \dots \right] \sin(3\theta) + \left[3C_{3,c} r^2 - \frac{5}{16} C_{3,c}^{[2]} r^4 + \dots \right] \cos(3\theta) + \\
& + \left[4C_{4,s} r^3 - \frac{3}{10} C_{4,s}^{[2]} r^5 + \dots \right] \sin(4\theta) + \left[4C_{4,c} r^3 - \frac{3}{10} C_{4,c}^{[2]} r^5 + \dots \right] \cos(4\theta) + \\
& + \left[5C_{5,s} r^4 - \dots \right] \sin(5\theta) + \left[5C_{5,c} r^4 - \dots \right] \cos(5\theta) + \\
& + \left[6C_{6,s} r^5 - \dots \right] \sin(6\theta) + \left[6C_{6,c} r^5 - \dots \right] \cos(6\theta) + \\
& + \dots
\end{aligned}$$

$$\begin{aligned}
B_\theta = & \left[C_{1,s} - \frac{1}{8} C_{1,s}^{[2]} r^2 + \frac{1}{192} C_{1,s}^{[4]} r^4 - \dots \right] \cos(\theta) - \left[C_{1,c} - \frac{1}{8} C_{1,c}^{[2]} r^2 + \frac{1}{192} C_{1,c}^{[4]} r^4 - \dots \right] \sin(\theta) + \\
& + \left[2C_{2,s} r - \frac{1}{6} C_{2,s}^{[2]} r^3 + \frac{1}{192} C_{2,s}^{[4]} r^5 - \dots \right] \cos(2\theta) - \left[2C_{2,c} r - \frac{1}{6} C_{2,c}^{[2]} r^3 + \frac{1}{192} C_{2,c}^{[4]} r^5 - \dots \right] \sin(2\theta) + \\
& + \left[3C_{3,s} r^2 - \frac{3}{16} C_{3,s}^{[2]} r^4 + \dots \right] \cos(3\theta) - \left[3C_{3,c} r^2 - \frac{3}{16} C_{3,c}^{[2]} r^4 + \dots \right] \sin(3\theta) + \\
& + \left[4C_{4,s} r^3 - \frac{1}{5} C_{4,s}^{[2]} r^5 + \dots \right] \cos(4\theta) - \left[4C_{4,c} r^3 - \frac{1}{5} C_{4,c}^{[2]} r^5 + \dots \right] \sin(4\theta) + \\
& + \left[5C_{5,s} r^4 - \dots \right] \cos(5\theta) - \left[5C_{5,c} r^4 - \dots \right] \sin(5\theta) + \\
& + \left[6C_{6,s} r^5 - \dots \right] \cos(6\theta) - \left[6C_{6,c} r^5 - \dots \right] \sin(6\theta) + \\
& + \dots
\end{aligned}$$

$$\begin{aligned}
B_z = & [C_0^{[1]} - \frac{1}{4}C_0^{[3]}r^2 + \frac{1}{64}C_0^{[5]}r^4 - \dots] + \\
& + [C_{1,s}^{[1]}r - \frac{1}{8}C_{1,s}^{[3]}r^3 + \frac{1}{192}C_{1,s}^{[5]}r^5 - \dots] \sin(\theta) + [C_{1,c}^{[1]}r - \frac{1}{8}C_{1,c}^{[3]}r^3 + \frac{1}{192}C_{1,c}^{[5]}r^5 - \dots] \cos(\theta) + \\
& + [C_{2,s}^{[1]}r^2 - \frac{1}{12}C_{2,s}^{[3]}r^4 + \dots] \sin(2\theta) + [C_{2,c}^{[1]}r^2 - \frac{1}{12}C_{2,c}^{[3]}r^4 + \dots] \cos(2\theta) + \\
& + [C_{3,s}^{[1]}r^3 - \frac{1}{16}C_{3,s}^{[3]}r^5 + \dots] \sin(3\theta) + [C_{3,c}^{[1]}r^3 - \frac{1}{16}C_{3,c}^{[3]}r^5 + \dots] \cos(3\theta) + \\
& + [C_{4,s}^{[1]}r^4 - \dots] \sin(4\theta) + [C_{4,c}^{[1]}r^4 - \dots] \cos(4\theta) + \\
& + [C_{5,s}^{[1]}r^5 - \dots] \sin(5\theta) + [C_{5,c}^{[1]}r^5 - \dots] \cos(5\theta) + \\
& + \dots
\end{aligned}$$

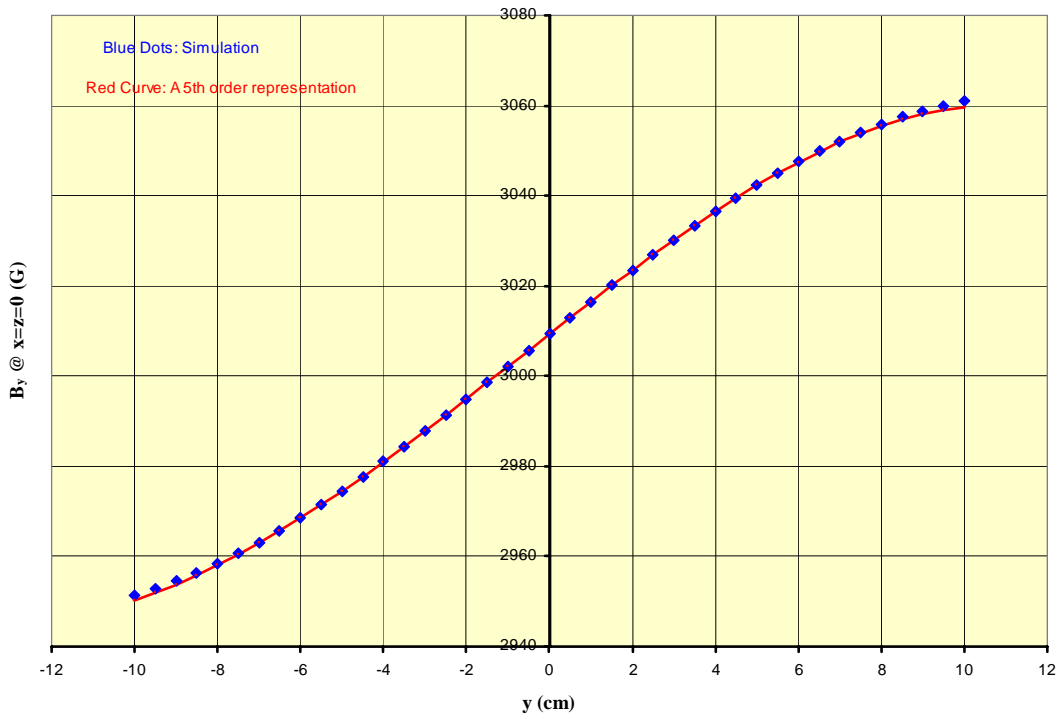


Fig. 11 B_y versus y at x=z=0.

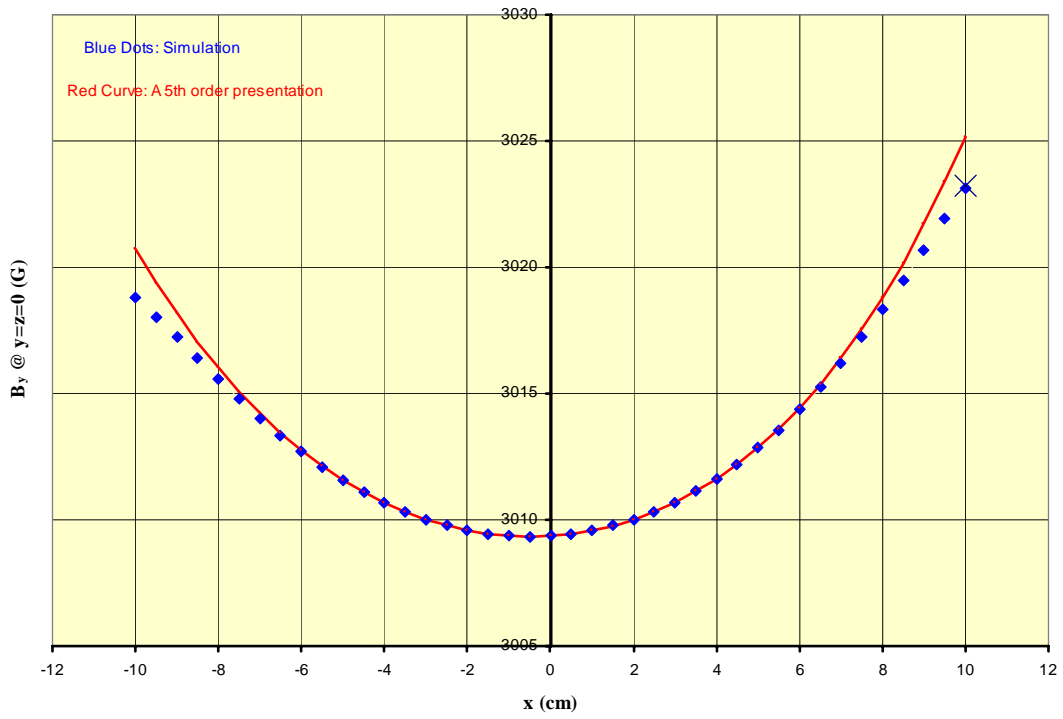


Fig. 12 B_y versus x at y=z=0.

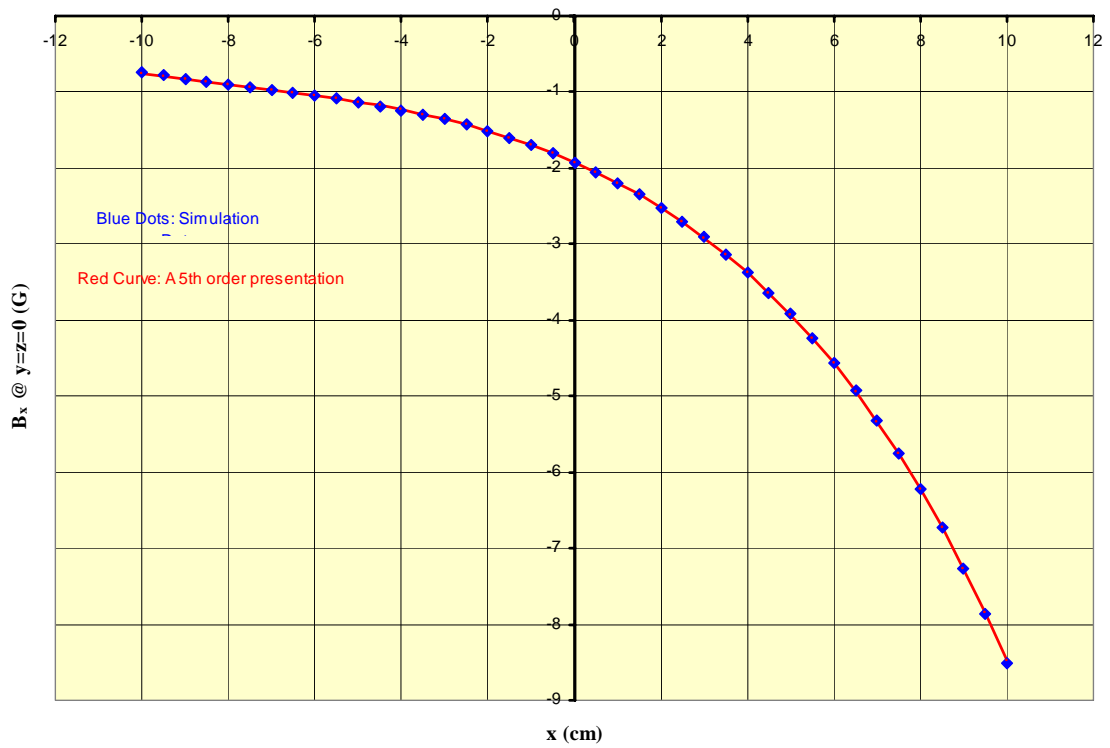


Fig. 13 B_x versus x at y=z=0.

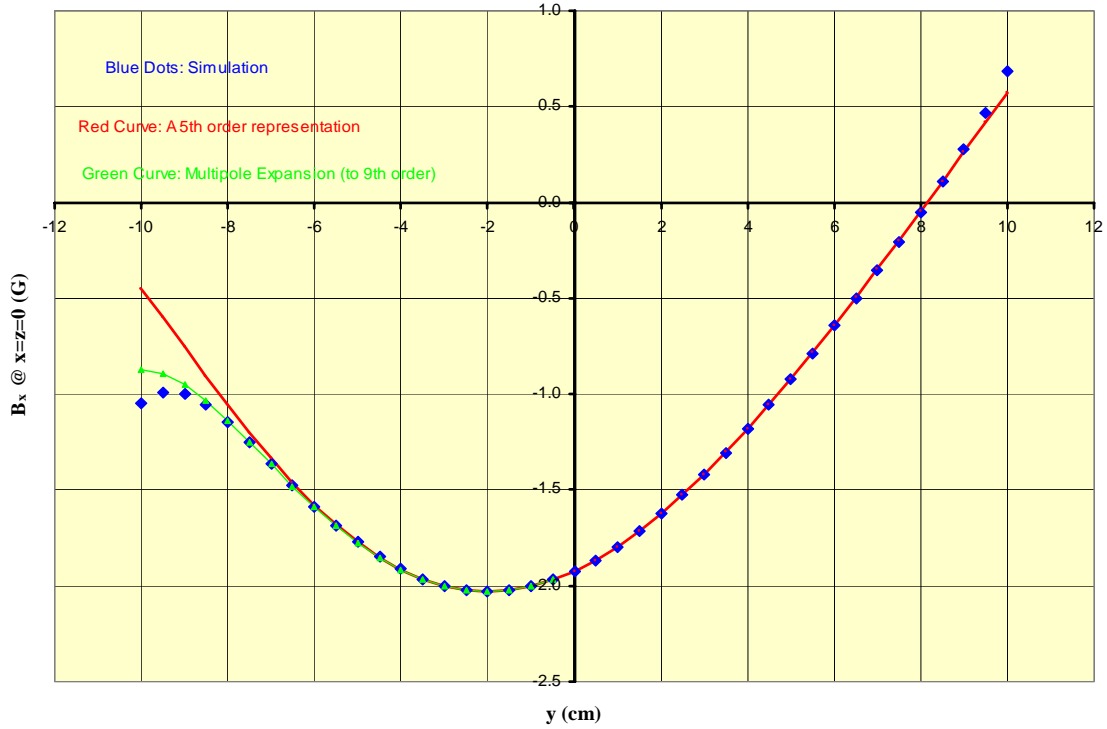


Fig. 14 B_x versus y at $x=z=0$.

4. Magnetic fringe fields and interferences in ring doublets

The SNS ring employs in its straight sections closely packed quadrupole doublet magnets [7, 8] plus dipole correctors. As shown in Fig. 15, the quadrupole doublet magnets (30Q58 & 30Q44) have large aperture of $R=15.1$ cm and relatively short iron-to-iron distance of 51.4 cm. The dipole corrector (41CD30) is only 21.4 cm away from 30Q58 iron core. These quads have much extended fringe fields, and magnetic interferences among the magnets in the doublet assemblies are not avoidable. Though each quad is measured individually at high accuracy of 10^{-4} level, there is no experimental measurement of the magnet interference effect in the assemblies. This causes concerns about the performance characteristics of the doublets, and about commissioning and operation of the ring. We have performed 3D computer simulations on a quadrupole doublet model in order to investigate the effect of magnetic fringe fields, to assess the degree of the interferences, and to obtain relevant data which should be very useful for the SNS ring commissioning and operation [9].

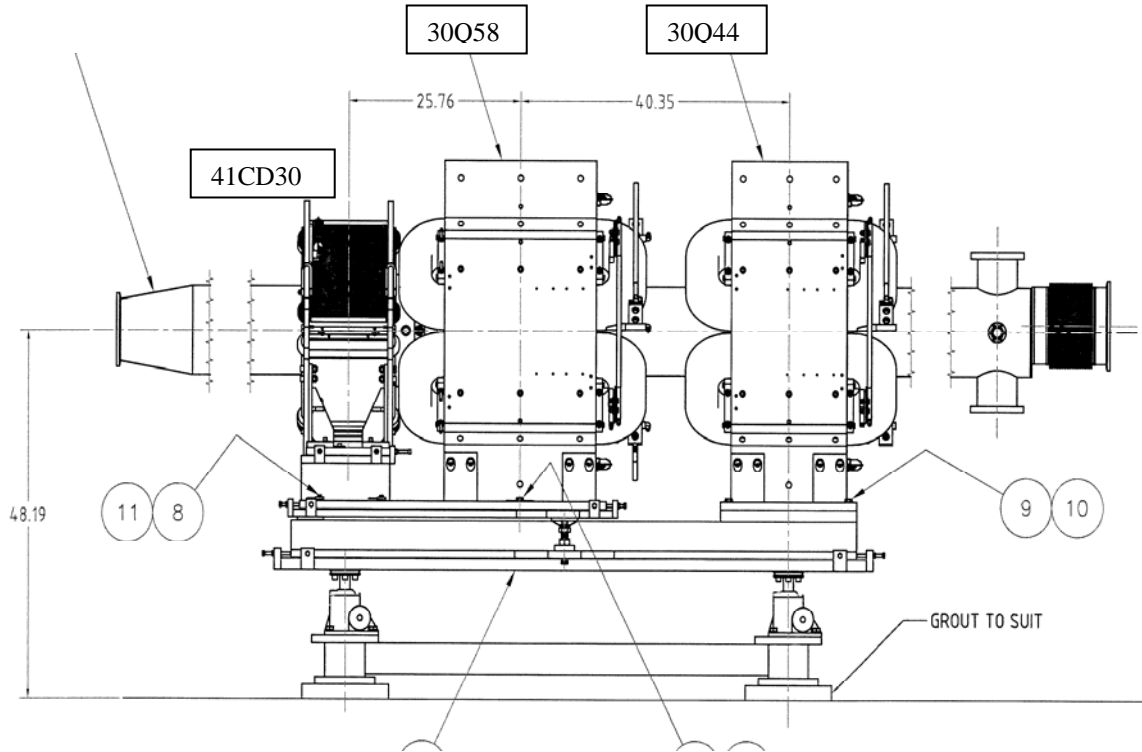


Fig. 15 SNS ring doublet assembly [10].

We have first simulated 30Q58 and 30Q44 separately. The models are built with the OPERA3d package “Modeller”. In the simulation the currents are 810 A and -860 A for 30Q58 and 30Q44, respectively, which are close to their operation points for 1 GeV beam energy. We then combine the two magnets together in simulation. This results in the magnetic interference between the two quads in the doublet. Finally, we add the iron core of 41CD30 in modeling. The simulation with two quads yields an output file of about 1.6 GB in memory. It is very slow to do this with a PC. Figure 16 shows the final simulation model with three magnets. In Fig. 17 we plot the magnetic field component B_y at $x=10$ cm and $y=0$ as a function of the axial position z for three cases: the dark blue curve represents the field of 30Q58 alone; the light blue curve shows the field of 30Q44 itself; the red curve is the field when the three magnets are together in simulation. It is obvious that the integrated fields, as well as the integrated gradient, get smaller for each magnet in the assembly than that when they stand alone due to the magnetic interferences. The quantitative reduction in the integrated gradients due to the interferences is shown in Table 2. In calculations we employ a rotating, rectangular patch of $r_4=14.224$ cm and $r_2=-7.112$ cm, which is similar to the un-bucked winding of a Halbach coil in measurements [11].

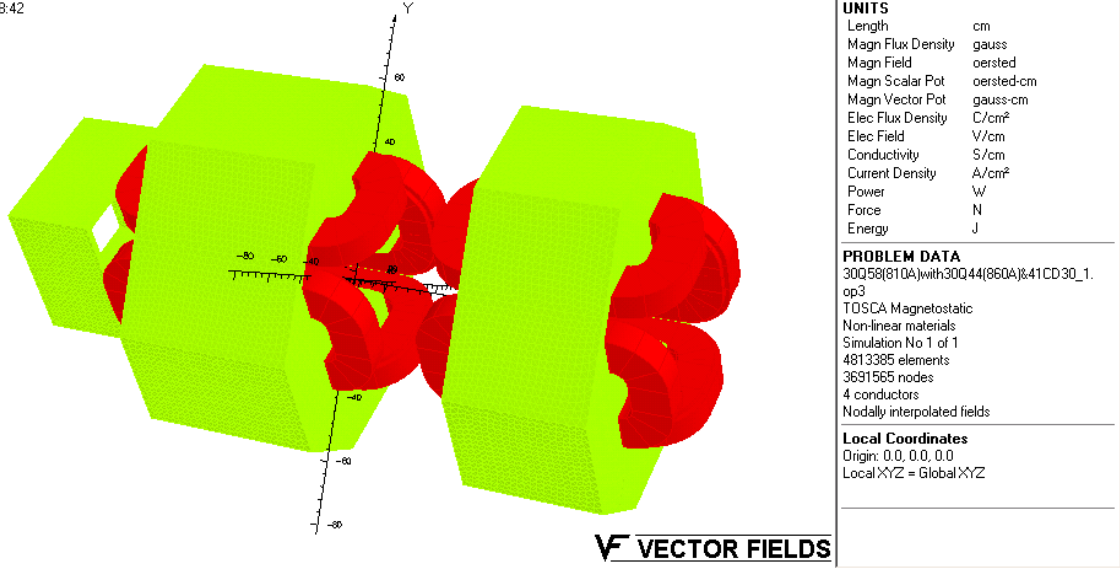


Fig. 16 Simulation model for SNS ring doublet magnets (30Q58 & 30Q44 plus 41CD30 core).

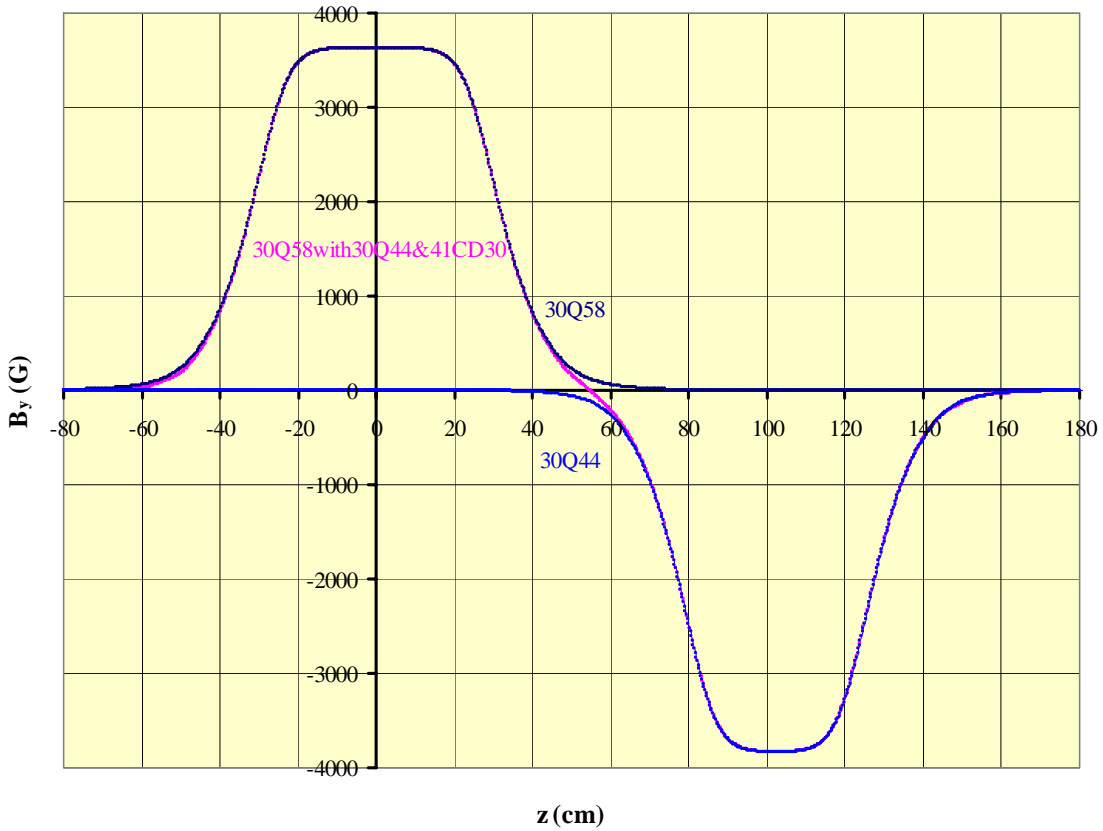


Fig. 17 Magnetic field B_y at $x=10$ cm & $y=0$ versus z for SNS ring doublet assembly.

Table 2 Changes in integrated gradients

	<u>30Q58</u>	<u>30Q44</u>
<u>As Singlet:</u>	2.4597 (T)	2.0721 (T)
<u>In Doublet:</u>	2.4434 (T)	2.0555 (T)
(Reduction):	(0.66%)	(0.80%)
<u>In Assembly:</u>	2.4311 (T)	2.0550 (T)
(Reduction):	(1.16%)	(0.83%)

5. Summary

Computing 3D-simulations of quite a few SNS magnets have been performed at ORNL. We have found that the simulations are very useful and beneficial for the SNS magnet measurements on site. Based on simulation data a 3D multipole expansion can be made, that not only reveals interesting magnet physics but also serves the basis for further beam optics analyses. The simulation of the magnetic fringe fields and interferences in the SNS ring straight section assembly yields alarming results: the integrated gradient of 30Q58 would be reduced by more than 1% due to its neighbors. This probably is the largest magnetic interferences in the SNS ring, and is worth further detailed investigation. We believe that continuous effort in 3D simulations of the SNS ring magnets has now become the major option to answer the remaining questions of the SNS ring magnets and related beam dynamics issues during commissioning and operation.

Acknowledgements

The author would like to thank T. Hunter for his support of 3D magnet simulation activities in our tasks. We also would like to acknowledge W. Meng and N. Tsoupas of BNL for their assistance in simulations of the injection chicane dipoles and the ring narrow quads for the doublets. All the magnet dimensions in our simulations are taken from the BNL/SNS design drawings available on the web site [10]. We appreciate J. Simkin of Vector Field, England, for his help in many details of the OPERA code and simulation technique.

References

- [1] OPERA-3d (an **OP**erating environment for **E**lectromagnetic **R**esearch and **A**nalysis) is the pre and post processing system for electromagnetic analysis programs such as TOSCA (for non-linear magneto static or electrostatic field and current flow problems) developed by Vector Fields Limited, England.
- [2] J. G. Wang, T. Hunter, D. LeBon, and R. McBrien, "CHARACTERIZATION OF A SNS TRANSFER LINE DIPOLE", SNS-Notes-MAG 0070, May 31, 2002, also in Proceedings of EPAC2002, pp.2388-2390, Paris, France, June 3-7, 2002.
- [3] J. G. Wang, "Field Non-uniformity of SNS HEBT Dipoles", SNS-NOTE-MAG 0081, September 6, 2002.
- [4] J. G. Wang, "Final Test Results of SNS HEBT Dipoles", SNS-NOTE-MAG-0110, July 25, 2003.
- [5] D. T. Abell, Y. Y. Lee, W. Meng, in Proc. of EPAC 2000, p. 2107.
- [6] J. G. Wang, "Field Distribution of Injection Chicane Dipoles (D2 & D3) on SNS Ring", SNS-NOTE-MAG-130, September 1, 2004, also submitted to the 2005 Particle Accelerator Conference, Knoxville, TN, May 16-20, 2005.
- [7] N. Tsoupas, et al., "A Large-aperture Narrow Quadrupole for the SNS Accumulator Ring", in Proc. EPAC 2002, p.1106, Paris, June 3-7, 2002.
- [8] N. Tsoupas, et al., "Magnetic Field Calculations for a Large Aperture Narrow Quadrupole", in Proc. PAC 2003, Portland, Oregon, May 12-16, 2003
- [9] J. G. Wang, N. Tsoupas, and M. Venturini, "3D Simulation Studies of SNS Ring Doublet Magnets", submitted to the 2005 Particle Accelerator Conference, Knoxville, TN, May 16-20, 2005.
- [10] <http://dwg-server.c-ad.bnl.gov/eng-arch/source.htm>
- [11] K. Halbach, "The Hilac Quadrupole Measurement Equipment", Engineering Note, LBL, March 3, 1972.